Chronic imaging and manipulation of cells and vessels through a polished and reinforced thinned-skull

Patrick J. Drew[1,2,3], **Andy Y. Shih**[1], **Jonathan D. Driscoll**[1], **Per Magne Knutsen**[1], **Pablo Blinder**[1], **Dimitrios Davalos**[4], **Katerina Akassoglou**[4,5], **Philbert S. Tsai**[1], and **David Kleinfeld**[1,6,7]

[1] Department of Physics, University of California at San Diego, CA

[2] Center for Neural Engineering, Department of Engineering Science and Mechanics, The Pennsylvania State University, University Park, PA

[3] Department of Neurosurgery, The Pennsylvania State University, University Park, PA

[4] Gladstone Institute of Neurological Disease, University of California, San Francisco, CA

[5] Department of Neurology, University of California, San Francisco, CA

[6] Graduate Program in Neurosciences, University of California at San Diego, CA

[7] Center for Neural Circuits and Behavior, University of California at San Diego, CA

Abstract

We present a method to form an optical window in the mouse skull that spans millimeters and is stable for months without inflammation of the brain. This enabled us to repeatedly image blood flow in cortical capillaries of awake animals and determine long-range correlations in speed. We further demonstrate repeated cortical imaging of dendritic spines, microglia, and angioarchitecture, as well as illumination to drive motor output via optogenetics and induce microstrokes via photosensitizers.

Keywords

Microscopy; Imaging; Neuroscience

Chronic observation and manipulation of cells in the cortex is integral to studies on neurons, glia, and microvasculature. An increasingly popular application involves the use of *in vivo*

two-photon laser scanning microscopy (TPLSM) to image deep within mammalian cortex through a window in the skull[1]. This may be formed by a craniotomy[2], in which a section of skull is removed and replaced with glass, or by thinning a section of the skull with a microsurgical blade[3]. Both methods have been employed for the chronic observation of fluorescently labeled neuronal processes[3,4] and microvasculature[5], yet have limitations. It has been suggested that cranial windows activate microglia and astrocytes as part of an inflammatory response[6] that can alter neuronal physiology[7] and pial blood vessels[8], although these complications may relate to surgical finesse[9]. The thinned skull procedure avoids the activation of microglia and astrocytes[6], yet access is limited to a very small area, *i.e.*, ~ 0.2 mm^2 compared with 1 to 10mm^2 for a craniotomy. Further, sequential imaging sessions require re-thinning of the skull to counteract re-growth of the bone, which limits the number of times that imaging can be performed and leaves the area under the thinned portion of skull mechanically vulnerable[3]. Thus there is a need for a technique that provides readily available optical access across a large area of the brain without the potential to induce inflammation.

We introduce a polished and reinforced thinned-skull (PoRTS) procedure to create a large, chronically stable window in the skull. We attempt to satisfy four goals with this method: (1) Optical clarity, sufficient for imaging with TPLSM as well as optogenetic control, without the need to intervene after the initial surgery; (2) Optical access across many square millimeters; (3) Mechanical stability for imaging in awake animals; and (4) The absence of an inflammatory response.

Our basic idea is to mechanically thin the skull[3], polish the cut surface to improve flatness, then use transparent cement and glass to form a clear, rigid window that is fused to the thinned bone. The glass window is designed to stabilize the thinned and thus weakened bone, and both the mechanical stability and the fusion of the window to the bone is reasoned to inhibit regrowth of bone, thus preserving clarity. In detail, the skull is thinned with a high speed burr to a final thickness of 10 to 15 μm, polished without direct pressure on the skull with a slurry of grit in artificial cerebral spinal fluid (ACSF), and then fused to a cover glass with a thin layer of cyanoacrylate cement (Fig. 1A).

The optical transfer function for two-photon excited fluorescence measured through the PoRTS window is modestly degraded compared to that found using only a cover glass (Fig. 1B). The resolution varies across the window, presumably as a result of natural inhomogeneities in bone, with a radial width of 0.7 to 1.0 μm (full width of half of the integrated intensity) and an axial resolution of about 3 μm. Further, the TPLSM signal is diminished by a factor of $e^{-1.5}$ by the thinned bone (Supplementary Fig. 1); this is equivalent to the loss in signal by imaging through 150 μm of brain tissue[10]. Despite such caveats, we could repeatedly observe the dendritic spines of neurons that express yellow fluorescent protein (YFP) both two days and several weeks after surgery (2 animals) (Fig. 1C). Second, we repeatedly imaged subsurface brain microvessels in animals in which the plasma was stained with fluorophore-conjugated-dextran. Good visibility was obtained up to 250 μm below the pial surface for periods up to three months (35 animals) (Fig. 1D). In a more stringent examination, we found that the pattern of subsurface microvascular architecture was stable when the same group of microvessels was imaged over a period of

40 days through a PoRTS window (3 fields across 2 animals) (Fig. 1E). Consistent with the long-term optical clarity of subsurface brain structures, the PoRTS window appears to impede regrowth of the thinned skull as assayed by measuring the thickness of the skull over time (Supplementary Fig. 2).

A critical biological assessment of the PoRTS window concerns the potential activation of microglia; these cells change their morphology in response to insults to the brain[11]. We utilized transgenic mice that express enhanced green fluorescent protein (EGFP) in microglia, *i.e.*, line *Cx3cr1eGFP+/−*. At two days after surgery, which corresponds to the time when microglia are maximally active under a craniotomy[6], we observe a diffuse, highly branched morphology of microglia under the PoRTS window that is indicative of non-activation (3 animals) (Supplementary Fig. 3). An essentially identical pattern is seen on the control, contralateral hemisphere. Submicrometer microglial processes, at depths greater than 100 μm below the surface, were readily imaged over a period of two months (Supplementary Fig. 4). Repeated imaging of the same general area showed a continued absence of activated microglia up to at least one month following installation of the PoRTS window (5 animals at 2 days, 3 animals at 14 days, and 3 animals at 30 days) (Supplementary Fig. 5).

A further assessment concerns reporters of brain trauma as evaluated within the area of cortex just below the PoRTS window. First, we assessed the expression of glial fibrillary acidic protein (GFAP), which is up-regulated in reactive astrocytes during brain injury[12]. The pattern of immunostaining for GFAP was found to be weak and indistinguishable from that seen on the control, contralateral hemisphere (3 animals) (Supplementary Fig. 6). This implies a lack of astrocyte activation. Second, we exploited the past finding that cortical injury can trigger remodeling and outgrowth of surface pial vasculature[8]. We observe that the pial surface vasculature remains nearly unchanged (2 fields in each of 2 animals) with the PoRTS window (Supplementary Fig. 7). *In toto*, the astrocyte, microglia and vascular data show that the PoRTS window does not induce a classic inflammatory response in the brain. By contrast, companion experiments reveal an increase in the density of brightly immunostained GFAP-positive reactive astrocytes below a craniotomy (3 animals), as well as an alteration of the topology of the vasculature (2 animals) that occurs primarily through the growth of surface veins following a craniotomy (Supplementary Fig. 7).

An application that exploits the large area of cortex that is visible through the PoRTS concerns the possibility of long-range correlations in vasomotion[10], a 0.1 to 1 Hz oscillation in vascular tone that is hypothesized to be part of the "default" state of brain activity[13]. We made simultaneous measurements of the flow of red blood cells (RBCs) in pairs of subsurface microvessels, defined as vessels with diameters less than 7.5 μm, in awake animals. The RBCs can be measured in vessels over 100 μm below the pial surface and separated by up to 500 μm (17 animals measured up to 60 days after implantation of the window) (Fig. 2A-D). As a population, the baseline speed was heterogeneous (0.90 ± 0.61 mm/sec; mean $\pm$ SD; 159 vessels) (Supplementary Fig. 8) and matches the values found for anesthetized rat[10]. Of critical interest, low-frequency variations in blood flow were strongly and significantly correlated out to 500 μm (Fig. 2E), the longest separation we could probe. Coherence at the heart rate, which serves as a positive control, was strongest

between microvessels separated by less than 100 μm and remained significant out to 500 μm, Intermediate frequencies showed considerably less coherence. These data provides direct evidence for high spatial coherence of the 0.1 to 1.0 Hz vasomotion in awake animals.

We now turn to the manipulation of brain activity. A first application concerns the excitation of neurons expressing light-sensitive channels through the PoRTS window. We used a strain of mice that express channelrhodopsin-2 (ChR2) in the layer 5 pyramidal neurons, *i.e.*, thy–1–YFP–-ChR2, and found that vibrissa movements were elicited by illumination of motor cortex with blue light (2 awake animals) (Fig. 3A,B). This shows that focal excitation of cells that express ChR2 is compatible with the PoRTS window. As a second application, we show that we can induce microstrokes via photosensitizers through the PoRTS window. An optically-mediated occlusion to a single penetrating arteriole, the vessel that sources blood from the cortical surface to the paranchyma, is induced by focal illumination of the photosensitizer Rose-Bengal, which circulates intravenously, with green laser light. This leads to a localized clot (2 animals) (Fig. 3C,D). Occlusion of this single vessel is sufficient to produce a significant infarct (Fig. 3E), as seen previously with a craniotomy[14]. Use of the PoRTS window permits the effects of experimental stroke on cortical viability to be characterized while avoiding the possibility of additional damage from the craniotomy procedure. Overall, these examples show the utility of the PoRTS window for physiological manipulation as well as imaging.

In summary, the PoRTS method enables high resolution chronic imaging and optical manipulation through large windows into the brain for periods of at least three months. The windows do not require regular maintenance, do not induce an apparent inflammatory response nor lead to vascular rearrangement, and may be used with awake animals. The downside of imaging through thinned bone is a loss in resolution, although this may be ameliorated through the use of adaptive optics to correct for distortions of the wave-front of the incident excitation beam. Lastly, the PoRTS window may be combined with miniaturized, head mounted microscopes for chronic imaging in free-ranging animals[15].

Supplementary Material

Refer to Web version on PubMed Central for supplementary material.

Acknowledgments

Abbreviations

ACSF   Artificial cerebral spinal fluid

ChR2	Channelrhodopsin-2
eGFP	Enhanced green fluorescent protein
GFAP	Glial fibrillary acidic protein
PoRTS	Polished and reinforced thinned-skull
RBC	Red blood cell
TPLSM	Two photon laser scanning microscopy
YFP	Yellow fluorescent protein

References

1. Svoboda K, Denk W, Kleinfeld D, Tank DW. Nature. 1997; 385:161. [PubMed: 8990119]

2. Levasseur JE, Wei EP, Raper AJ, Kontos AA, Patterson JL. Stroke. 1975; 6:308. [PubMed: 1154467]

3. Grutzendler J, Kasthuri N, Gan WB. Nature. 2002; 420:812. [PubMed: 12490949]

4. Trachtenberg JT, Chen BE, Knott GW, Feng G, Sanes JR, Welker E, Svoboda K. Nature. 2002; 420:788. [PubMed: 12490942]

5. Brown CE, Li P, Boyd JD, Delaney KR, Murphy TH. Journal of Neuroscience. 2007; 27:4101. [PubMed: 17428988]

6. Xu HT, Pan F, Yang G, Gan WB. Nature Neuroscience. 2007; 10:549. [PubMed: 17417634]

7. Hauss-Wegrzyniak B, Lynch MA, Vraniak PD, Wenk GL. Experimental Neurology. 2002; 176:336. [PubMed: 12359175]

8. Sohler TP, Lothrop GN, Forbes HS. Journal of Pharmacology and Experimental Therapeutics. 1941; 71:325.

9. Holtmaat A, Bonhoeffer T, Chow DK, Chuckowree J, De Paola V, Hofer SB, Hubener M, Keck T, Knott G, Lee WC, Mostany R, Mrsic-Flogel TD, Nedivi E, Portera-Cailliau C, Svoboda K, Trachtenberg JT, Wilbrecht L. Nature Protocols. 2009; 4:1128. [PubMed: 19617885]

10. Kleinfeld D, Mitra PP, Helmchen F, Denk W. Proceedings of the National Academy of Sciences USA. 1998; 95:15741.

11. Stoll G, Jander S. Progress in Neurobiology. 1999; 58:233. [PubMed: 10341362]

12. Pekny M, Nilsson M. Glia. 2005; 50:427. [PubMed: 15846805]

13. Fox MD, Raichle ME. Nature Reviews of Neuroscience. 2007; 8:700. [PubMed: 17704812]

14. Blinder* P, Shih* AY, Rafie CA, Kleinfeld D. Proceedings of the National Academy of Sciences USA. 2010; 107:12670.

15. Sawinski J, Wallace DJ, Greenberg DS, Grossmann S, Denk W, Kerr JND. Proceedings of the National Academy of Sciences USA. 2009; 106:19557.

16. Jung S, Aliberti A, Graemmel P, Sunshine MJ, Kreutzberg GW, Sher A, Littman DR. Molecular and Cellular Biology. 2000; 20:4106. [PubMed: 10805752]

17. Arenkiel BR, Peca J, Davison IG, Feliciano C, Deisseroth K, Augustine GJ, Ehlers MD, Feng G. Neuron. 2007; 54:205. [PubMed: 17442243]

18. Frostig RD, Dory Y, Kwon MC, Masino SA. Proceedings of the National Academy of Sciences USA. 1993; 90:9998.

19. Stosiek C, Garaschuk O, Holthoff K, Konnerth A. Proceedings of the National Academy of Sciences USA. 2003; 100:7319.

20. Kleinfeld D, Delaney KR. Journal of Comparative Neurology. 1996; 375:89. [PubMed: 8913895]

21. Denk W, Delaney KR, Kleinfeld D, Strowbridge B, Tank DW, Yuste R. Journal of Neuroscience Methods. 1994; 54:151. [PubMed: 7869748]

22. Tsai, PS.; Kleinfeld, D. Methods for In Vivo Optical Imaging, 2nd edition. Frostig, RD., editor. CRC Press; Boca Raton: 2009. p. 59

23. Tsai PS, Friedman B, Ifarraguerri AI, Thompson BD, Lev-Ram V, Schaffer CB, Xiong Q, Tsien RY, Squier JA, Kleinfeld D. Neuron. 2003; 39:27. [PubMed: 12848930]

24. Nguyen, Q-T.; Dolnick, EM.; Driscoll, J.; Kleinfeld, D. Methods for In Vivo Optical Imaging. 2. Frostig, RD., editor. CRC Press; Boca Raton: 2009. p. 117

25. Nguyen QT, Tsai PS, Kleinfeld D. Journal of Neuroscience Methods. 2006; 156:351. [PubMed: 16621010]

26. Shih AY, Friedman B, Drew PJ, Tsai PS, Lyden PD, Kleinfeld D. Journal of Cerebral Blood Flow and Metabolism. 2009; 29:738. [PubMed: 19174826]

27. Shih, AY.; Nishimura, N.; Nguyen, J.; Friedman, B.; Lyden, PD.; Schaffer, CB.; Kleinfeld, D. Imaging in Neuroscience and Development. Yuste, R., editor. Vol. 2. Cold Spring Harbor Laboratory Press; New York: 2009. in press

28. Valmianski I, Shih AY, Driscoll J, Matthews DM, Freund Y, Kleinfeld D. Journal of Neurophysiology. 2010; 104:1803. [PubMed: 20610792]

29. Drew PJ, Blinder P, Cauwenberghs G, Shih AY, Kleinfeld D. Journal of Computational Neuroscience. 2010; 29:5. [PubMed: 19459038]

30. McMenamin PG. Journal of Comparitive Neurology. 1999; 405:553.

31. Ferezou I, Haiss F, Gentet LJ, Aronoff R, Weber B, Petersen CCH. Neuron. 2007; 56:907. [PubMed: 18054865]

32. Knutsen PM, Derdikman D, Ahissar E. Journal of Neurophysiology. 2005; 93:2294. [PubMed: 15563552]

33. Nishimura N, Schaffer CB, Friedman B, Lyden PD, Kleinfeld D. Proceedings of the National Academy of Sciences USA. 2007; 104:365.

34. Born, M.; Wolf, E. Principles of Optics: Electromagnetic Theory of Propagation Interference and Diffraction of Light. 6. Pergamon Press; Oxford: 1980.
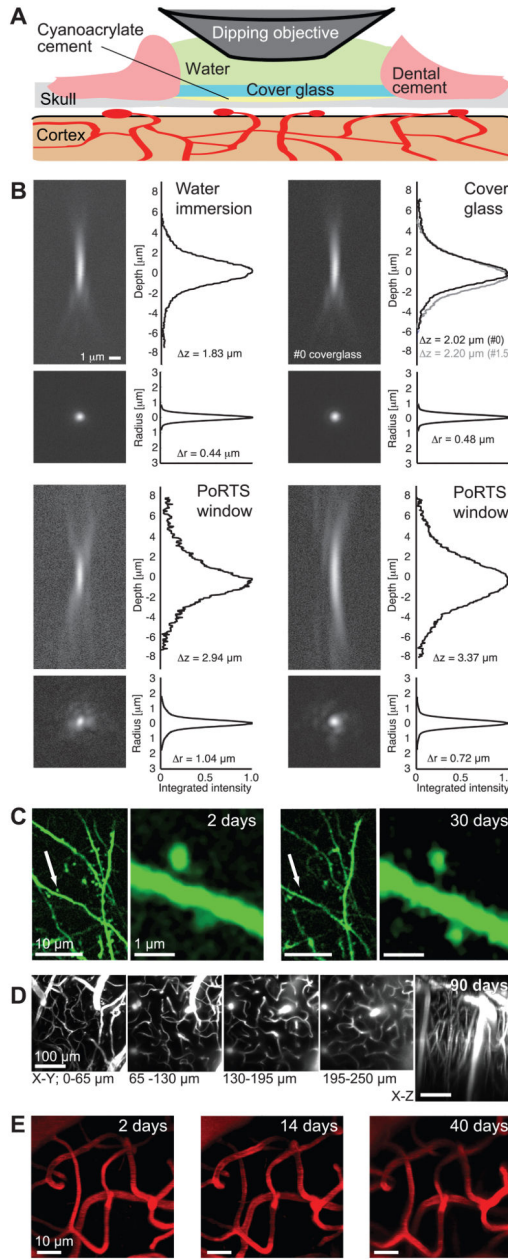
Figure 1. PoRTS window procedure, optical properties, and basic capabilities
(A) Schematic of the window. The thinned and polished skull is protected with a cover glass attached with cyanoacrylate cement. Dental cement is used to seal the edge of the cover glass and provide support for the meniscus. The thinned area is typically 1 – 2 mm on edge.
(B) Point spread functions for TPLSM determined by imaging 0.2 µm fluorescent beads were embedded in 1 % (w/v) agarose and imaged with a 40x, 0.8 NA water dipping objective. The axial depth profile shown the integrated radial intensity along the optical axis, *i.e.*, z-axis, and the radial depth profile shows the integrated axial intensity along the radial axis. The reported z and r are the full widths that encompass half of the integrated intensity. The top left panel shows a bead imaged through only water along width depth

profiles. The top right panel shows a bead imaged under a #0 cover glass (black line) along with depth profiles, along with the profiles for a #1.5 cover glass (grey line). The two bottom panels show separate examples of beads imaged through an excised PoRTS window. **(C)** Dendrites and spines of thy1-YFP expressing neurons two days (left panel) and 30 days (right panel) after PoRTS window implantation. Images were taken 30 μm below the surface. Reduction in the brightness of the YFP over time necessitated averaging of five frames for images taken one month after implantation; the dwell time was 6 μs per pixel and the average incident power was 35 – 70 mW. Representative image from a set of two mice **(D)** Maximum z-axis projections across 65 μm of fluorescein-conjugated-dextran filled vasculature through a PoRTS window 90 days after surgery. Each image is the average of six frames, the z-step was 2 μm, the dwell time was 3 μs per pixel and the average power was 25 – 120 mW. Representative images from a pool of 35 mice **(E)** Subsurface microvessels are stable under the PoRTS window for over a month after implantation. Images show maximum projections across 20 – 70 μm below the surface using an average of 5 frames, a dwell time of 6 μs per pixel, and an average power of 30 – 45 mW. Representative images from a set of two mice.
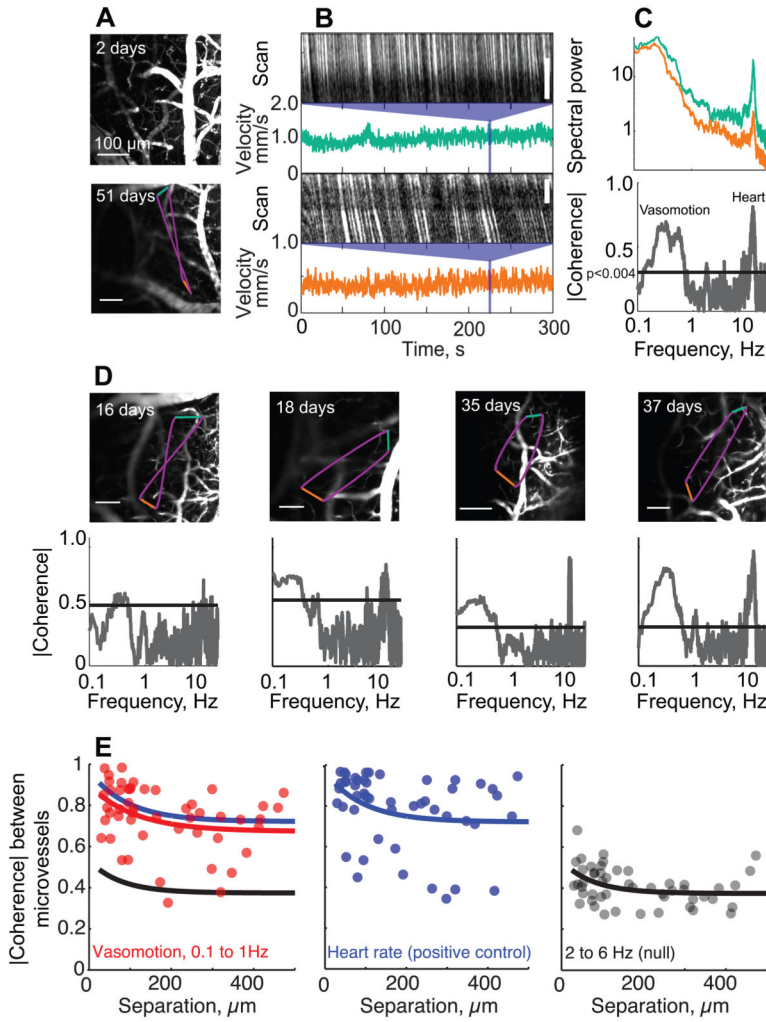
Figure 2. Long-range coherence of the velocity of RBC flow in capillaries in the cortex of awake head-fixed mice through a PoRTS window

Example data in panels A to D **are** taken from the same animal using a 10x,0.3 NA lens and averaging over 5 – 10 frames (**A**) Top panel is the maximal z projection over 90 μm of images of fluorescein-conjugated-dextran labeled vasculature, based on frames separated by 10 μm, two days after surgery. Bottom panel is an image from a single plane in the same animal, but a different location, 51 days after surgery. The colored lines show the scan path of the laser focus: green and orange are constant velocity segments along capillaries and purple are minimum time segments between capillaries. (**B**) Space-time plots of one segment of line scan data for each of two capillaries, with the calculated instantaneous velocity for the entire 300 s run shown below. (**C**) Top panel shows power spectra for the two velocity traces in panel B; 0.083 Hz bandwidth. A rhythmic component at ~ 10 Hz results from the heartbeat. Bottom panel is the magnitude of the spectral coherence between the velocities of the two capillaries as a function of frequency; 0.1 Hz bandwidth. Line denotes a significance of p < 0.004, which corresponds to the inverse of twice the number of degrees of freedom. Note the strong coherence at the heart rate and at the 0.1 – 1 Hz vasomotor frequencies. (**D**) Examples of spontaneous velocity coherences between

capillaries obtained various times after surgery; 0.1 Hz bandwidth. Panels A-D show representative data from a pool of 17 animals monitored up to 60 days after implantation **(E)** The coherence as a function of distance (50 vessel pairs in 9 mice). Left panel is the mean coherence in the 0.1 – 1.0 Hz vasomotor band. Center panel is the coherence at the heart-rate, which serves as a positive control for the maximum possible coherence. Right panel is the coherence in the 2 to 6Hz band, which serves as the null hypothesis. Colored lines correspond to fits with exponential functions to the corresponding spectral band.
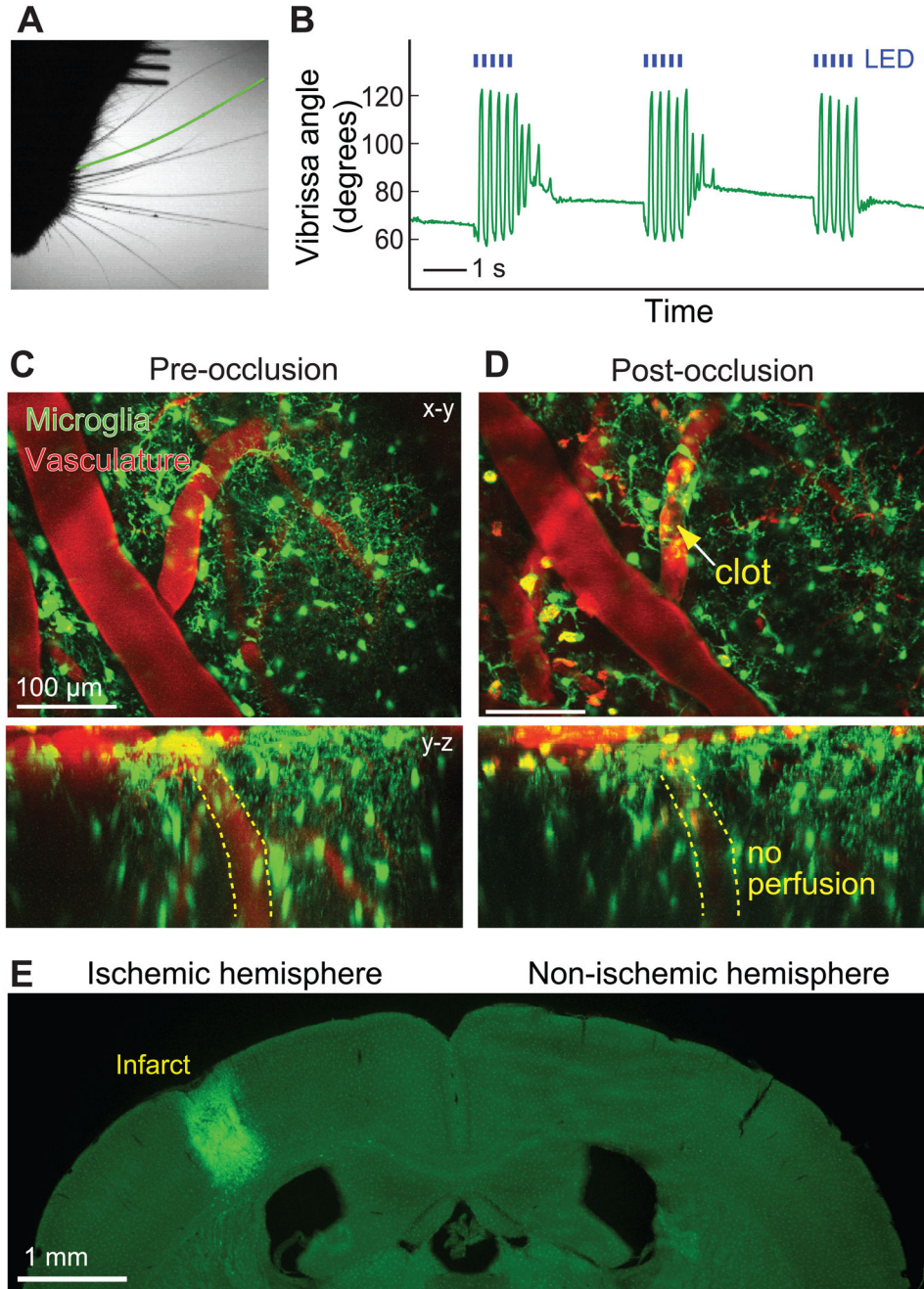
Figure 3. Examples of cortical physiology evoked through the PoRTS window
(**A**) Sample frame from video of awake, head-fixed ChR2 carrying mouse with a PoRTS window fabricated over vibrissa motor cortex 150 days earlier. Green line marks the position of the caudal vibrissa that is tracked over time. (**B**) Rostral-caudal motion of a caudal vibrissa in response to pulses of 467 nm light (5 Hz, 100 ms pulse duration; blue lines) from a light emitting diode (LED). Larger angles indicate retraction. A-B representative data from a set of two animals. (**C and D**) Maximal projection (x-y and y-z) through a 200 μm depth of a *Cx3cr1$^{eGFP+/-}$* mouse cortex before (panel C) and 100 minutes

after (panel D) occlusion of a single penetrating arteriole using targeted optical activation of Rose Bengal (yellow arrow points to clot). Images are averages of four frames with a dwell time of 3 μs per pixel and 1 μm steps along the z-axis. Note the change in microglia morphology to an amoeboid shape around the occluded arteriole and the interruption of flow as evidenced by the absence of Texas Red in the penetrating vessel highlighted in the y – z projection in the bottom pannels. The occlusion was made one day after implantation of the window. **(E)** The extent of the infarct, for the same animal as in panels C and D, visualized two days after the optically generated stroke. Note the invasion of eGFP labeled microglia into the cyst. The data in panels C to E are representative images from a set of two mice.